

Scaling laws for direct laser acceleration in a radiation-reaction dominated regime

M. Jirka,^{1,2} M. Vranic,³ T. Grismayer,³ and L. O. Silva³

¹*Institute of Physics of the Czech Academy of Sciences,
ELI Beamlines, Na Slovance 2, 182 21 Prague, Czech Republic*

²*Faculty of Nuclear Sciences and Physical Engineering,
Czech Technical University in Prague, Brehova 7, 115 19 Prague, Czech Republic*

³*GoLP/Instituto de Plasmas e Fusão Nuclear, Instituto Superior Técnico,
Universidade de Lisboa, Lisbon, 1049-001, Portugal*

We study electron acceleration within a sub-critical plasma channel irradiated by an ultra-intense laser pulse ($a_0 > 100$ or $I > 10^{22}$ W/cm²). In this regime, radiation reaction significantly alters the electron dynamics. This has an effect not only on the maximum attainable electron energy but also on the phase-matching process between betatron motion and electron oscillations in the laser field. Our study encompasses analytical description, test-particle calculations and 2-dimensional particle-in-cell simulations. We show single-stage electron acceleration to multi-GeV energies within a 0.5 mm-long channel and provide guidelines how to obtain energies beyond 10 GeV using optimal initial configurations. We present the required conditions in a form of explicit analytical scaling laws that can be applied to plan the future electron acceleration experiments.

In the interaction of under-dense plasma with a strong laser pulse, plasma electrons can be accelerated to relativistic velocities [1]. Depending on the laser pulse duration, different mechanisms are responsible for electron acceleration. Using laser-wakefield acceleration (LWFA) technique, one can obtain quasi-monenergetic electron energy distribution [2–5]. The highest electron energy achieved in experiments with LWFA to-date is 7.8 GeV [6]. For an efficient LWFA, the laser pulse duration τ_0 should be on the order of $1/\omega_p$, where ω_p is the electron plasma frequency. Short lasers ($\tau_0 \sim 30$ fs) are required to achieve this.

For a long laser pulse $\tau_0 \gg 1/\omega_p$, where LWFA is not efficient, an alternative acceleration mechanism can be explored. Upon laser propagation through the underdense plasma, the ponderomotive force expels electrons sideways resulting in the formation of a positively charged plasma channel. The formation of longitudinal plasma wave used for particle acceleration in LWFA is prevented by the length of the laser pulse. However, the formation of long-range transverse fields is still possible, due to the charge displacement and the electron current. Electrons propagating at relativistic velocities aligned with the channel axis undergo betatron oscillations, similarly as in LWFA bubble regime. At the same time, they are also experiencing the transverse laser fields. If the frequency of betatron oscillations is close to the Doppler-shifted laser frequency, then the laser energy can be efficiently coupled to the electron (so-called betatron resonance). This regime of electron acceleration is referred to as the direct laser acceleration (DLA) [7]. The rich physics of this setup has raised a keen interest among researchers in the past few years [8–25]. It was reported that the efficiency of DLA may be enhanced using various strategies: parametric amplification of betatron oscillations [26–29], applying additional longitudinal electric field [30, 31] or by "breaking of the adiabaticity

that precludes electron energy retention" [32]. Even a few DLA experiments have been performed using weakly relativistic laser intensities [33, 34].

Ultra-intense laser beams will become available through the next generation of 10 PW-class laser systems [35–37]. Interaction with a very intense pulse can provide a strong acceleration through DLA, but the underlying physics becomes even more complex than before. Relativistic electrons in a strong electromagnetic field lose energy by radiation, which in turn alters their trajectories. [38]. This phenomenon is called radiation reaction (RR) and is expected to affect electron motions at laser intensities exceeding 10^{22} W/cm². A small local change in electron trajectory can make a difference as to whether the betatron resonance is achieved by that electron or not [29]. It is therefore necessary to assess the effect of radiation reaction on DLA for the lasers of ultra-high intensities, i.e. when $a_0 \gtrsim 100$, where a_0 is the dimensionless normalized vector potential defined by $a_0 \simeq 86 \sqrt{I_0 [10^{22} \text{W/cm}^2]} \lambda_0 [\mu\text{m}]$, with I_0 and λ_0 representing the laser intensity and wavelength respectively.

The question regarding the role of radiation reaction in DLA was addressed in several recent works. The studies encompass the effect of radiation reaction on the formation of an ultradense helical electron bunch [39, 40] and emission of γ -rays [41, 42]. Somewhat counter-intuitively, radiation damping can be favourable for particle acceleration. One way to contribute is through allowing particle trapping near the channel axis in situations where all electrons would be expelled if no radiation was emitted. The trapped electrons interact with the peak laser intensity and can potentially achieve multi-GeV energies [43–45]. Another way to contribute is through the change of resonant conditions. Even though radiation reaction may reduce the global maximum achievable energy of accelerated electrons, it can strongly enhance acceleration of some electrons [46].

Obtaining a precise description of DLA is a challenge even without considering radiation reaction. By extending the mathematical tools previously developed for classical relativistic DLA at moderate laser intensities ($a_0 \lesssim 10$) [18], this paper aims to pave the path for a quantitative description of DLA including radiation reaction. In particular, we explore how RR changes the onset of betatron resonance and provide analytical predictions for the final electron energy. We discuss different aspects that affect or limit the acceleration, and find the promising parameter ranges and scaling laws to guide future experiments. The laws are verified with a comprehensive numerical study, involving test particles in ideal conditions, as well as full-scale self-consistent 2D particle-in-cell simulations. The setup considered in this work is a pre-formed plasma channel irradiated by an intense laser pulse that accelerates plasma electrons which are initially at rest (somewhere within the channel or at the channel walls). Our findings show that a fraction of particles that can achieve the betatron resonance is greatly increased by RR, which allows for high charge content in the accelerated electron beam. We quantify which are the necessary initial conditions and expected asymptotic energies for those particles.

This manuscript is organized as follows. In section I, we provide the analytical description of electron dynamics within a plasma channel in the presence of an intense laser field. We consider cases with and without radiation reaction in a simplified field configuration. In section II, test particle simulations are presented, the obtained data are compared with the analytical predictions, and the validity of used approximations is verified. Section III features 2D Particle-In-Cell (PIC) simulations with a pre-formed plasma channel, while the summary of the work is given in section IV.

I. ELECTRON DYNAMICS IN A PLASMA CHANNEL WITH A LASER FIELD

In this section, we analyze the acceleration of a single electron in a symmetric plasma channel irradiated by an ultra-intense linearly polarized laser. Using DLA scheme, the electron can be efficiently accelerated only if it achieves the betatron resonance. Whether this condition is fulfilled depends on initial conditions of the electron (e.g. distance from the axis, initial momentum, etc.) and the background plasma density. In addition, as the electron performs betatron oscillations in a strong electromagnetic background field, it loses its energy by emitting photons which, in turn, alters its dynamics [38]. All these effects have an impact on achieving the betatron resonance, and thus on the overall dynamics of the electrons within the plasma channel.

We first introduce our configuration and an analytical description of a particle performing the coupled oscillations.

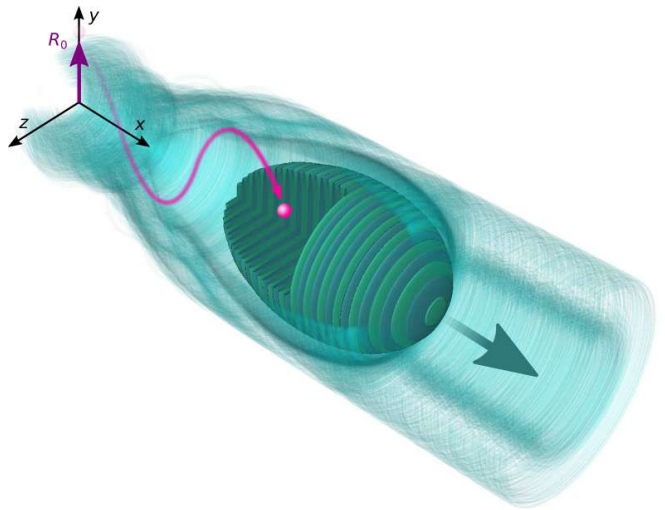


FIG. 1. Simulation setup: an intense laser pulse accelerates an electron in a cylindrically symmetric plasma channel.

This motion has an invariant \mathcal{I} that can be used to obtain the resonance condition. The next step is to estimate how much energy particles can gain over a certain acceleration distance, still without radiation reaction. We show later on that the principal effect of radiation reaction is to limit to the maximum energy achievable on a resonant trajectory. More specifically, radiation reaction breaks the invariant \mathcal{I} and it is possible to quantify this change over a resonant cycle. A decrease in \mathcal{I} results in a gradual change of the resonant condition over time, which allows the electron to become resonant even if its initial conditions were far from optimal.

Integral of motion in simplified electromagnetic configuration

A rigorous analytical description of our setup requires a few simplifications. Similarly as in previous works, in this section we consider the laser to be a plane wave, and the channel fields to be a linear function of the distance from the propagation axis x [18, 19, 27]. Consequently, the channel fields are radially symmetric with respect to the x -axis. The electron can be placed initially at different radial positions inside the plasma channel or on channel walls (see figure 1). We consider electrons starting at rest, and in the (x, y) plane (the plane defined by the laser polarisation and propagation direction). The laser propagates in positive x direction and the fields are given by $\mathbf{E}_L = E_0 \sin \phi \hat{\mathbf{y}}$, $\mathbf{B}_L = B_0 \sin \phi \hat{\mathbf{z}}$, where E_0 and B_0 are the amplitudes of the electric and magnetic field and ϕ is the phase of the wave. The phase velocity of the laser is assumed to be equal to the speed of light c , which is justified by the low plasma density and high laser intensity (this is verified in section II).

The electromagnetic field experienced by the electron is the combination of the laser field and the fields emerging due to the displacement of plasma electrons in the channel (channel fields) [7]. These self-generated quasi-static channel fields are the radial electric field and the azimuthal magnetic field

$$\mathbf{E}_C = f \frac{m_e \omega_p^2}{2e} \mathbf{r}, \quad \mathbf{B}_C = (1-f) \frac{m_e \omega_p^2}{2ec} \mathbf{r} \times \mathbf{v}, \quad (1)$$

where $\mathbf{r} = y \hat{\mathbf{y}} + z \hat{\mathbf{z}}$ is perpendicular to the channel axis and $\mathbf{v} = v \hat{\mathbf{x}}$ is the velocity of the flow. The numerical factor f depends on the fraction of electrons within the plasma channel and takes values between $0 \leq f \leq 1$ [17–19, 21, 26, 29]. The transversely expelled electrons generate the radial electric field, while electrons accelerated forward within the channel form a current that generates the azimuthal magnetic field. Usually, the higher the background plasma density, the lower the value of f [44]. In other words, the channel fields are linearly dependent on a radial distance from the channel axis, but the electric field E_C and the magnetic field B_C do not necessarily have the same magnitude. The total electromagnetic field experienced by the electron is then given by

$$\mathbf{E} = \mathbf{E}_L + \mathbf{E}_C, \quad \mathbf{B} = \mathbf{B}_L + \mathbf{B}_C. \quad (2)$$

The field structure defined in equation (2) induces electron oscillations due to the laser field as well as betatron oscillations at the same time. The background plasma density n_p affects the electron motion since the magnitude of the self-generated channel fields is proportional to the plasma frequency: $\omega_p^2 = 4\pi e^2 n_p / m_e$. We, therefore, expect DLA to be sensitive to the initial conditions of the electron, the intensity of the laser pulse and the density within the plasma channel.

Without radiation reaction, the electron motion in the channel is only governed by the Lorentz force:

$$\frac{d\mathbf{p}}{dt} = -e \left(\mathbf{E} + \frac{\mathbf{p}}{\gamma m_e c} \times \mathbf{B} \right), \quad (3)$$

where $\gamma = \sqrt{1 + (|\mathbf{p}|/m_e c)^2}$ is the relativistic Lorentz factor and \mathbf{p} is the electron momentum. For particles propagating in the positive x -direction, both \mathbf{E}_C and \mathbf{B}_C contribute in a similar manner: they provide a restoring force that pushes electrons towards the channel axis. In fact, the value of the numerical factor f from equation (1) is not important because the restoring force is actually proportional to $|\mathbf{E}_C| + |\mathbf{B}_C|$.

From the Hamiltonian of the electron, one obtains an integral of motion \mathcal{I} . For a particle that is initially in the (x, y) plane with $z = 0$, the integral of motion can be written as [18]

$$\mathcal{I} = \gamma - \frac{p_x}{m_e c} + \frac{\omega_p^2 y^2}{4c^2}, \quad (4)$$

where p_x is the component of the electron momentum in the direction of wave propagation. For a better intuitive understanding, it is useful to note that the first two terms of the integral of motion are the same as for the particle interacting with a plane wave in vacuum, while the third term accounts for the transverse harmonic oscillations within the channel. The value of \mathcal{I} defines a limit on the energy attainable in the system if all dissipation mechanisms are neglected. For example, in the case of the electron initially at rest placed on the channel axis ($y = 0$), the value of the integral of motion is $\mathcal{I} = 1$ [18].

Betatron resonance

Due to the interaction with the channel fields, the electrons perform betatron oscillations with the frequency given by $\omega_\beta = \omega_p / \sqrt{2\gamma}$ [47]. We define the betatron period to be $T_\beta = 2\pi / \omega_\beta$. For electrons propagating in the same direction as the laser, the frequency of the quiver motion due to the laser field depends on how fast the electron moves in the x -direction. If the velocity of the electron is v_x while the laser propagates at approximately the speed of light c (underdense plasma) the Doppler-shifted laser frequency can be expressed as $\omega_L = \omega_0 (1 - v_x/c)$. The electron in the channel can achieve an efficient acceleration if the conditions for the betatron resonance are met, i.e. when the Doppler-shifted laser frequency ω_L is close to the betatron frequency [7]

$$\omega_L \simeq \omega_\beta. \quad (5)$$

If we assume that the momentum of an ultra-relativistic electron accelerated in the channel is predominantly pointing in the forward direction ($p_x \gg p_y \gg m_e c$), then the forward momentum can be expressed [18] as $p_x \simeq \gamma m_e c [1 - (1/2) (p_y / \gamma m_e c)^2]$. After replacing p_x into equation (4), we obtain [25]

$$\mathcal{I} \simeq \frac{1}{2\gamma} \left(\frac{p_y}{m_e c} \right)^2 + \frac{\omega_p^2 R^2}{4c^2}. \quad (6)$$

Equation (6) allows to obtain an expression for $p_y \simeq m_e c \sqrt{2\gamma \mathcal{I}} \cos \psi$, where the amplitude of the oscillations is written as $y = R = R_0 \sin \psi$, and ψ is the betatron phase. The Doppler-shifted laser frequency is now

$$\omega_L \simeq \omega_0 \frac{\mathcal{I}}{\gamma} \cos^2 \psi. \quad (7)$$

The resonant condition $\omega_L \simeq \omega_\beta$ applies to an average over the entire cycle, and not for the instantaneous values of ψ . For the condition to be satisfied, the required particle energy is

$$\gamma^* \approx 2\mathcal{I}^2 \left(\frac{\omega_0}{\omega_p} \right)^2 \cos^4 \psi. \quad (8)$$

\mathcal{I} being an invariant, we can also write $\mathcal{I} = \mathcal{I}_0$ and $\mathcal{I}_0 = 1 + [\omega_p R_0 / (2c)]^2$ for a particle initially at rest. This means that the maximum γ_{\max}^* and average $\langle \gamma^* \rangle$ in a resonant cycle can be expressed as

$$\gamma_{\max}^* \simeq 2\mathcal{I}^2 \left(\frac{\omega_0}{\omega_p} \right)^2, \quad \langle \gamma^* \rangle \simeq \frac{3}{4}\mathcal{I}^2 \left(\frac{\omega_0}{\omega_p} \right)^2, \quad (9)$$

using cycle-averaged value $\langle \cos^4 \psi \rangle = 3/8$. According to equation (9), the resonant electron energy does not depend on the laser intensity but solely on the initial position and the background plasma density. However, the intensity will determine how long it may take an electron to get accelerated towards the resonant energy. In the next subsection, we will discuss the work of the electromagnetic field for optimal particle acceleration, with a special consideration of resonant electrons.

Optimal acceleration for quasi-resonant electrons

The work performed by the electric field of the laser on one particle is given by $dW = -e \int \mathbf{E} \cdot \mathbf{p} / (\gamma m_e) dt$. In our configuration, the fields are purely transverse and only the p_y component is relevant

$$\frac{dW}{dt} \simeq -eE_0 c \sqrt{\frac{2\mathcal{I}}{\gamma}} \sin \phi \cos \psi. \quad (10)$$

This expression is composed of two oscillatory functions. It is therefore crucial to determine under which conditions the averaged work does not vanish. Intuitively, the initial phase of the particle should be favourable and the oscillation frequencies should be of the same order. This can be understood by looking at figure 2. The field is doing constructive work when \mathbf{p}_y is anti-parallel with \mathbf{E}_L . If $T_L \ll T_\beta$, then during one betatron oscillation, there are many oscillations of the laser field whose work in the positive and negative half-cycles would cancel making the total work vanish. By approximating the slowly varying function $\sin \psi$ as a step function, then at best we can obtain one entire laser cycle T_L of the constructive work within one T_β (sections of the cycle with constructive contribution are shaded in figure 2). This would give $\langle \sin \phi \cos \psi \rangle_{\max} \simeq \langle |\sin \phi| \rangle T_L / T_\beta \simeq (2/\pi) T_L / T_\beta$. If we apply the same idea, but account on average for the fact that betatron oscillations are not a step function, we get $\langle |\sin \phi \cos \psi| \rangle_{\max} \simeq (2/\pi)^2 T_L / T_\beta$. The work of the field is therefore expected to be less efficient when there is a large discrepancy between the oscillation periods T_L and T_β . Inserting our estimates into equation (10) and expressing the values of T_L and T_β as a function of \mathcal{I} , ω_0 , and ω_p , we can estimate the maximum attainable constructive power

$$\left\langle \left| \frac{dW}{dt} \right| \right\rangle \simeq \frac{8}{\pi^2} \frac{eE_0 c \omega_p}{\sqrt{\mathcal{I}} \omega_0}. \quad (11)$$

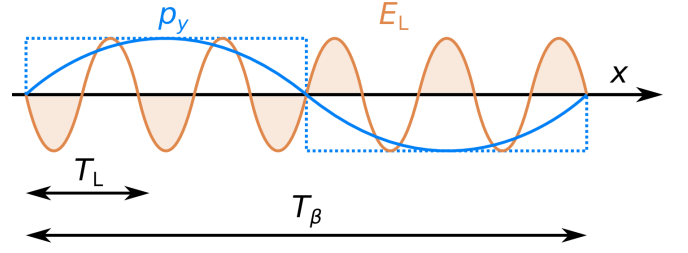


FIG. 2. Shaded regions illustrate constructive work of the laser field E_L acting on the electron with p_y within one betatron cycle T_β . T_L is the laser period. The dotted line represents the approximation of $\sin \psi$ as a step function.

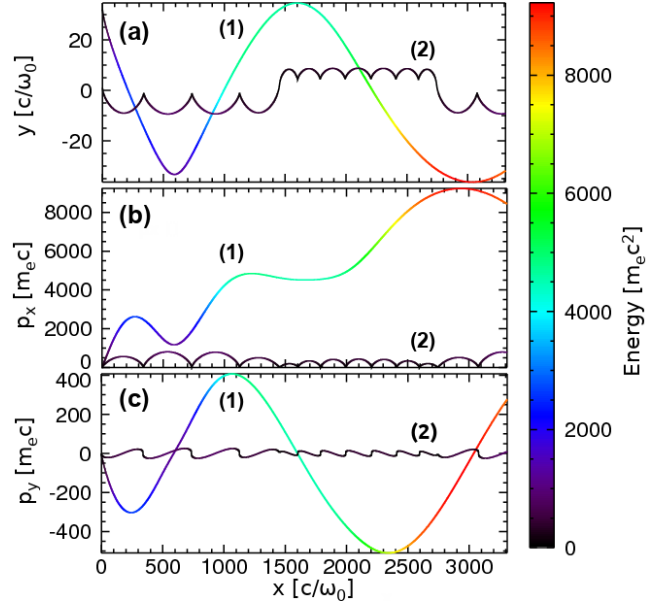


FIG. 3. (a) Electron trajectory, (b) longitudinal and (c) transverse momenta during the acceleration within a plasma channel where $\omega_p / \omega_0 = 0.5$ and for two different initial electron positions: (1) $R_0 = 28 c / \omega_0$ and (2) $R_0 = 0$. In both cases, the laser pulse has $a_0 = 100$. The color bar represents the relativistic γ factor of electrons.

This represents the power for the best case scenario — there is no guarantee that any particles would meet this condition. Figure 3 illustrates a resonant vs. non-resonant particle trajectory. It is clear that some particles never get accelerated, despite being in the strong field. A strict calculation would be possible for resonant particles for which $\langle \sin \phi \cos \psi \rangle_{\max} \simeq 1/2$. This yields a solution similar to what equation (11) predicts for $T_L \simeq T_\beta$.

Equation (11) considers the local amplitude of the electric field E_0 . As we are usually dealing with laser pulses, this local field will vary in space and time. We could assume, for example, a \sin^2 shape function for the laser temporal envelope. This would lower the total work done

by the laser from the beginning to the time when the particle gets to the highest field region approximately by a factor of two. From that we can derive the expected cut-off energy versus time

$$\mathcal{E}[\text{MeV}] \simeq 0.38 \frac{a_0}{\sqrt{\mathcal{I}}} \frac{\omega_p}{\omega_0} \frac{t[\text{fs}]}{\lambda_0[\mu\text{m}]} \quad (12)$$

which can also be presented as a function of the acceleration distance l_{acc}

$$\mathcal{E}[\text{MeV}] \simeq 1.27 \frac{a_0}{\sqrt{\mathcal{I}}} \frac{\omega_p}{\omega_0} \frac{l_{\text{acc}}}{\lambda_0}. \quad (13)$$

From (12) and (13), we observe that particles which start with a low \mathcal{I} can experience a more efficient acceleration. Moreover, their resonant γ is lower according to equation (9), so the resonance may be easier to achieve. Consequently, for any setup with a predetermined acceleration distance, we may have particles at a preferential initial \mathcal{I} to achieve the betatron resonance at a highest value of γ . We can then extract the value for the optimum initial distance from the channel axis

$$\frac{R_{\text{opt}}}{\lambda_0} = 0.4 \left(a_0 \frac{l_{\text{acc}}}{\lambda_0} \right)^{1/5} \left(\frac{\omega_0}{\omega_p} \right)^{2/5}. \quad (14)$$

The particles that were initially at the distance R_{opt} as defined by equation (14) have the best conditions for achieving the betatron resonance and getting accelerated. This remains true as long as the interaction is without radiation losses, i.e. the integral of motion is unchanged $\mathcal{I} \simeq \mathcal{I}_0$. We draw attention to the reader that the above calculations did not account for a transverse shape of the laser pulse, as the derivation considers a plane wave laser with a temporal envelope. However, one could extend

this model by using a lower effective a_0 to account for the transverse envelope function.

Effects of Radiation reaction

Radiation reaction must be present in addition to the Lorentz force to accurately resolve the motion of a particle when ultra-intense laser beams are considered. We model the radiation reaction term using the Landau-Lifshitz (LL) equation [38]

$$\frac{d\mathbf{p}}{dt} = -e \left(\mathbf{E} + \frac{\mathbf{p}}{\gamma m_e c} \times \mathbf{B} \right) + \mathbf{F}_{\text{RR}}, \quad (15)$$

where the leading order term of the radiation reaction force is given by

$$\mathbf{F}_{\text{RR}} = -\frac{2e^4}{3m_e^3 c^5} \gamma \mathbf{p} \left[\left(\mathbf{E} + \frac{\mathbf{p}}{\gamma m_e c} \times \mathbf{B} \right)^2 - \left(\frac{\mathbf{p}}{\gamma m_e c} \cdot \mathbf{E} \right)^2 \right]. \quad (16)$$

We mentioned before that the electron dynamics without radiation reaction does not depend on the value of f in equation (1) [21]. We will now show that even the radiation reaction force at the first order in \mathcal{I}/γ does not depend on the value of f . For simplicity, we assume again the laser to be a plane wave that is linearly polarized along the y -axis, and propagates along x . We consider an electron that starts in the plane $z = 0$ (in fact in the sub-plane $y > 0$ without loss of generality).

The electromagnetic fields experienced by the electron are given by equation (2), where E_C and B_C are positive by construction. The laser fields E_L and B_L can take any sign, but they are equal to one another in magnitude: $E_L = B_L = E_0 \sin \phi$. This field configuration cannot change p_z if it was initially zero, so the particle is confined in the (x, y) plane. We can simplify the term in square brackets of equation (16) considering the directions of \mathbf{E} and \mathbf{B} from equation (2) and replace p_x and p_y according to the previous values

$$\left(\mathbf{E} + \frac{\mathbf{p} \times \mathbf{B}}{\gamma m_e c} \right)^2 - \left(\frac{\mathbf{p} \cdot \mathbf{E}}{\gamma m_e c} \right)^2 \simeq \left(E_C + B_C + \frac{p_y^2}{2\gamma^2} E_L \right)^2 \simeq \left(E_C^* \sin \psi + \frac{\mathcal{I} \cos^2 \psi}{\gamma} E_0 \sin \phi \right)^2, \quad (17)$$

where

$$E_C^* \sin \psi = E_C + B_C \simeq \frac{m_e \omega_p^2}{2e} R. \quad (18)$$

We can draw an important conclusion from equation (17). In an extremely intense laser, it is likely to have $E_C^* \ll E_0$. However, even though E_C^* has a significantly smaller magnitude, the channel field dominates the radiation reaction as long as $E_0 \ll E_C^* \gamma / \mathcal{I}$. This inequality

can be violated for a large transverse momentum component $p_y \gg p_x$. It is not excluded that some particles could be in this situation before getting accelerated in the positive x -direction.

The energy loss can be approximated by

$$m_e c^2 \frac{d\gamma}{dt} \simeq -\alpha_{\text{RR}} \gamma^2 \left(E_C^* \sin \psi + \frac{\mathcal{I} \cos^2 \psi}{\gamma} E_0 \sin \phi \right)^2, \quad (19)$$

where $\alpha_{\text{RR}} = 2e^4/(3m_e^2 c^3)$ is the damping constant [38]. Radiation reaction sets a limit on the maximum electron energy attainable in the interaction with an ultra-intense laser pulse. The limit is reached when all the energy an electron can gain during one betatron cycle is radiated out during the same time interval. As a result, the particle energy is equal before and after such a cycle. In other words, no further acceleration is possible. For a relativistic particle that satisfies the condition $E_0 \ll E_C^* \gamma / \mathcal{I}$, we can estimate the maximum energy by equating $d\gamma/dt$ from equation (10) and equation (19) which leads to

$$\gamma_{\text{RR}} \approx \left(\frac{e^2 a_0 \omega_0}{\alpha_{\text{RR}} m \omega_p^2 \sqrt{2\mathcal{I}}} \right)^{2/5}. \quad (20)$$

Equation (20) represents the acceleration limit when the channel field is the dominant cause of radiation reaction and can be applied to quasi-resonant particles. The result can be simplified to

$$\gamma_{\text{RR}} \approx 1.484 \times 10^3 \left(\lambda_0 [\mu\text{m}] \frac{\omega_0^2}{\omega_p^2} \frac{a_0}{\sqrt{2\mathcal{I}}} \right)^{2/5}. \quad (21)$$

Radiation reaction-induced reduction of \mathcal{I}

When electrons lose energy due to radiation emission, the integral of motion \mathcal{I} defined in equation (4) is not conserved anymore. We can make a quantitative estimate of how \mathcal{I} changes during one resonant betatron cycle. Radiation losses change the instantaneous energy and momentum of the particles, which also reduces the integral of motion \mathcal{I} . For relativistic particles, we can assume that most of the radiation is emitted in the direction of motion (this emission is contained within a cone that has an opening angle $\theta \sim 1/\gamma$). According to this assumption, the momentum and energy are reduced proportionally: $d\gamma/\gamma \simeq dp/p \simeq dp_x/p_x$. The integral of motion therefore decreases through the reduction of $\gamma - p_x/(m_e c)$, in the following way:

$$d\mathcal{I} = d\gamma - \frac{dp_x}{m_e c} \simeq d\gamma \left(1 - \frac{p_x}{\gamma m_e c} \right), \quad (22)$$

where we used the proportionality mentioned above to express dp_x as a function of $d\gamma$. Using equation (22) we can derive that the integral of motion is reducing at a rate

$$\frac{d\mathcal{I}}{dt} = \frac{d\gamma}{dt} \frac{\mathcal{I} \cos^2 \psi}{\gamma}, \quad (23)$$

where $d\gamma/dt$ is given by equation (19).

We can estimate how much \mathcal{I} decreases during one resonant betatron cycle. We first perform a change of variables $dt = \gamma^*/(\mathcal{I} \cos^2 \psi) d\psi$, and use equation (8) to remove direct γ dependence. If we assume a limit where the channel field dominates, using $\int_0^{2\pi} \cos^8 \psi \sin^2 \psi d\psi = 7\pi/128$ we get \mathcal{I} decreases to

$$\mathcal{I} = \mathcal{I}_0 \left[1 + 3.2 \times 10^{-8} \frac{\omega_0^2}{\omega_p^2} \frac{\mathcal{I}_0^4}{\lambda_0 [\mu\text{m}]} \right]^{-1/4}. \quad (24)$$

In the other limit, where the laser field dominates, we have $\int_0^{2\pi} \cos^6 \psi d\psi = 5\pi/8$, which gives

$$\mathcal{I} = \mathcal{I}_0 \left[1 + 2.3 \times 10^{-8} a_0^2 \frac{\mathcal{I}_0}{\lambda_0 [\mu\text{m}]} \right]^{-1}. \quad (25)$$

Both equations (24) and (25) predict an asymptotic value that particles with a large initial value of \mathcal{I}_0 would tend to after a resonant cycle. If the predicted asymptotic \mathcal{I} is much smaller for one of the limits (RR due to the laser or due to the channel fields), it means that this limit represents the dominant contribution to the radiation reaction. As it turns out, the \mathcal{I} limit predicted by equation (24) is frequently lower than the one predicted by equation (25). An example for $a_0 = 500$ is given in figure 4. The figure illustrates that even one resonant betatron cycle can be enough to reduce the integral of motion very close to the value where the radiation reaction is not very strong anymore and cannot make a significant change during the subsequent cycles. Inserting the asymptotic value of \mathcal{I} into equation (21) will give us the maximum electron energy allowed due to the radiation reaction.

For predictions of the maximum energy in the system, one should compare equations (9), (13) and (21), using the lowest energy predicted among the three as a final result. One should consider the \mathcal{I}_0 for equation (13), because it applies to acceleration from the beginning of the interaction, while equations (9) and (21) should be considered with the value of \mathcal{I} reduced by radiation reaction.

II. TEST PARTICLE SIMULATIONS, COMPARISONS WITH THE ANALYTICAL MODEL

To validate our model and probe parameters optimal for particle acceleration, we now use a test-particle approach in a simplified electromagnetic configuration, similarly as in section I. We consider a wide range of initial conditions varying the particle distance from the channel axis, background plasma density and the laser intensity.

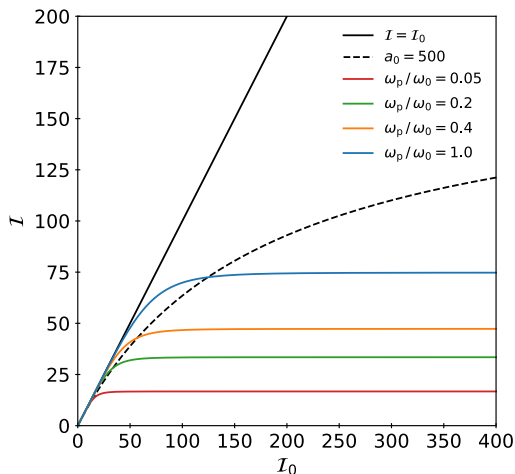


FIG. 4. Reduction of the invariant \mathcal{I} during one resonant betatron oscillation cycle. Dashed black line represents the prediction of equation (25) for a laser with $a_0 = 500$, while the coloured lines represent the predictions of equation (24) for different values of ω_p/ω_0 . For reference, $\mathcal{I} = \mathcal{I}_0$ is given as a solid black line.

This data can illustrate how limits presented in the previous section affect particle acceleration.

The laser is represented as a plane wave with a temporal envelope [21, 29], which propagates along the positive x direction at the speed of light and is polarised along the y -axis. We consider $\lambda_0 = 1 \mu\text{m}$ and a Gaussian temporal profile with duration $\tau = 150$ fs defined as full-width-at-half-maximum (FWHM) in the electromagnetic field amplitude. Due to the slowly-varying laser envelope function, the initial carrier-envelope phase does not impact the laser-electron interaction. The test particle equations of motion are integrated using the 4th order Runge–Kutta method with a time step $\Delta t = \lambda_0/(1000c)$ satisfying the condition for accurate calculation of electron dynamics in a strong laser field [48]. The numerical factor f introduced in equation (1) is here set to 0.5, such that the electric and magnetic field of the channel have an equal magnitude. The plasma channel is assumed to be axially symmetric, with a typical field structure given by equation (1). In our calculations, the length of the plasma channel is $528 \mu\text{m}$. In the following analysis, the distances are often expressed in units normalized to the laser frequency where $c/\omega_0 \approx 0.16 \mu\text{m}$. The electrons always start at rest at an initial distance R_0 from the channel axis. This corresponds to a case when an intense laser propagates through a pre-formed plasma channel and accelerates electrons originating from the channel walls. We vary R_0 from 0 to $100 c/\omega_0$ for different values of ω_p/ω_0 ranging from 0.01 to 1. For an optical laser, this corresponds to a plasma density range between 10^{17} and 10^{21} parts./ cm^3 , and distance from the channel axis up to $\sim 15 \mu\text{m}$. Radius and ω_p/ω_0 are sampled with 100 values each, which makes for 10^4 test cases just by

varying these two parameters. We also consider several values of a_0 , with examples of strong and weak radiation reaction.

Without radiation reaction

Figure 5 summarizes the results obtained from test-particle simulations without radiation reaction for three different values of a_0 . Each data point represents the maximum achieved value of relativistic Lorentz factor γ of an electron as a function of the initial value for $\mathcal{I}_0 \omega_0/\omega_p$. Some particles achieve energies over 10 GeV, and many of them are resonant according to equation (8). This is verified in figure 5 where γ_{max}^* is shown as a black solid line, while cycle-averaged value $\langle \gamma^* \rangle$ is represented with a dashed line. Particles are resonant at different energies for different values of $\mathcal{I}_0 \omega_0/\omega_p$, and, as shown in section I, the resonance condition does not depend on the laser intensity. The asymptotic energy, therefore, has to be estimated by considering how much work towards particle acceleration the laser can invest during the available acceleration distance. According to equation (13), this limit is a function of a_0 , \mathcal{I}_0 and ω_p . The color-coded solid lines show the maximum possible electron energy for quasi-resonant particles given by equation (13) corresponding to the acceleration distance of $528 \mu\text{m}$. For a specific set of parameters a_0 and ω_p , the most favourable initial R_0 for acceleration is the one that allows to achieve the betatron resonance at a highest electron energy within the available acceleration distance. This optimal R_{opt} corresponds to the intersection between the dashed and the coloured solid curves in figure 5, and is given by equation (14). The acceleration is in principle possible even far from betatron resonance, with a slightly lower maximum allowed energy. However, as we have mentioned before, the probability for constructive work performed by the laser towards particle acceleration is low for high values of \mathcal{I}_0 , where $R_0 \gg R_{\text{opt}}$. The existence of an optimal initial radial position is better illustrated in figure 6, where panels (a) and (b) display the test electron maximum energy as a function of R_0 and ω_p/ω_0 for the same dataset summarized in figure 5. We can also see sudden jumps in the maximum achieved energy between points with similar parameters, which suggest a resonant nature of the acceleration mechanism, as highlighted in the previous works [7, 8].

Effects of radiation reaction

When considering extreme laser intensities, we expect radiation reaction to be important for the particle dynamics, and consequently for acceleration. This section addresses the radiation reaction effects. We present test

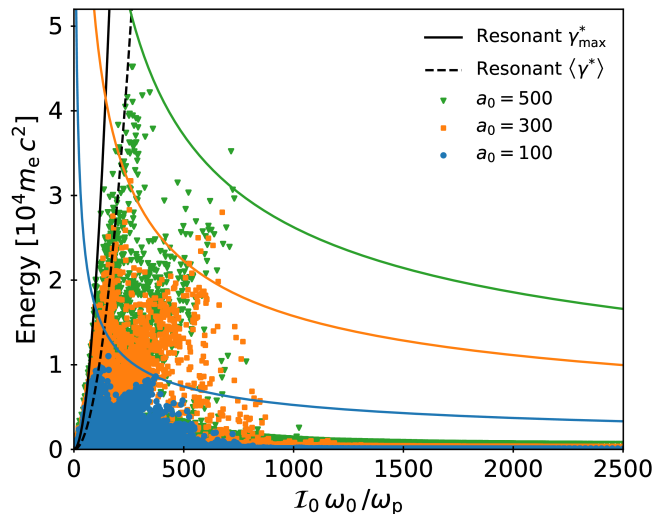


FIG. 5. Data points show the maximum value of electron energy as a function of the integral of motion \mathcal{I}_0 and the plasma frequency ω_p for different a_0 . In these runs, radiation reaction is neglected. Corresponding color-coded solid lines show the maximum electron energy according to equation (13) at the moment when the electron reaches the end of the channel. The black solid (dashed) line represents the analytical estimate of the maximum (cycle-averaged) electron energy given by the resonance condition (9).

particle simulations for the same parameters as in the previous section, but now including RR in the equations of motion. In the code, RR is implemented as a continuous process of losing electron energy described by the Landau-Lifshitz equation [38, 49]. We do not include the electron Gaunt factor correction in these simulations - we verify later in this section that this does not change our findings. The results of test-particle simulations for $a_0 = 100$ and $a_0 = 500$ are shown in figure 6 (c) and (d). The differences between cases with and without RR for $a_0 = 100$ are small, both in the absolute values of the energy obtained as well as in the parameters favourable to achieve betatron resonance. This suggests that RR is not strong for $a_0 = 100$. In contrast, the maximum energy achieved with RR is about a factor of two lower than without RR for $a_0 = 500$. But the most striking difference is in the parameter range where the maximum energy is achieved. It appears that all particles with $R_0 > R_{\text{opt}}$ can get accelerated. Since radiation reaction affects the electron dynamics and thus the evolution of the phase-matching process between the particle oscillations in the channel and the laser field, an efficient electron acceleration can be achieved for a wider range of initial conditions. This is accomplished through the reduction of the integral of motion, which allows particles with an initially large \mathcal{I}_0 to eventually converge to a lower quasi-resonant value of \mathcal{I} that enables energy retention.

We have compared the theoretical estimate for reduction of \mathcal{I} during one resonant cycle with the data ob-

tained from test-particle simulations. The predictions of equation (24) against the data for $a_0 = 500$ are shown in figure 7. The values of \mathcal{I} for our parameter range are restricted by three boundaries, as shown in figure 7 (a). The solid line represents a situation of weak radiation reaction where the integral of motion does not change. The dotted line corresponds to the highest plasma density we considered ($\omega_p/\omega_0 = 1$), while the dashed line is for electrons starting at the furthest initial position from the channel axes. Figure 7 (b) shows the integral of motion calculated from the data at the moment when the electron reaches its maximum energy. Equation (24) is a good predictor for the order of the final value of \mathcal{I} , even if we consider only one resonant betatron cycle. Some particles will have enough time to perform multiple betatron oscillations, and achieve the asymptotic value of \mathcal{I} where the radiation reaction becomes negligible. However, since this value is of the same order, for simplicity we will continue considering a single betatron cycle for computing the final \mathcal{I} . After inserting this corrected value of \mathcal{I} into equations (9) and (21), the equation that predicts a lower energy is a good estimate of the asymptotic energy of the electron, provided that the acceleration distance was long enough to achieve this energy according to equation (13).

We can verify this by presenting the test particle simulations with radiation reaction in a similar fashion as in figure 5. Figure 8 shows the maximum particle energy as a function of $\mathcal{I}_0 \omega_0/\omega_p$ for two different laser intensities, $a_0 = 400$ and $a_0 = 600$. If we assume that the electron is initially at the maximum distance $R_{\text{max}} = 100 c/\omega_0$ from the channel axis, then equation (21) provides the limit on the attainable electron energy which is illustrated by the dashed line in figure 8. The dotted line represents the expected value for $\omega_p = \omega_0$ according to equation (21). For $\omega_p/\omega_0 < 0.3$, there is a window of parameters that allows energies above 10 GeV. However, we do not see them in our results, because of the finite interaction time. As has been stated in the previous subsection, longer acceleration distance allows to accumulate more energy. This is illustrated in figure 9, where all parameters are kept equal, except the acceleration distance. The upper panels show the same plots as figure 7 for $a_0 = 500$ and $l_{\text{acc}} = 528 \mu\text{m}$ or $l_{\text{acc}} = 1056 \mu\text{m}$. The lower panels show the obtained energy vs. expected energy according to the minimum predicted by equations (9) and (21). There is a clear convergence of the data towards the maximum allowed energy we predict, but there are also outliers, especially for $\omega_p/\omega_0 < 0.3$. These particles do not attain their allowed maximum, either because there is not enough time, or because their initial integral of motion is already so low that the radiation reaction does not significantly affect their motion and they can easily remain far from the betatron resonance. A fraction of these particles eventually does converge towards the predicted values in the example with a longer propagation distance.

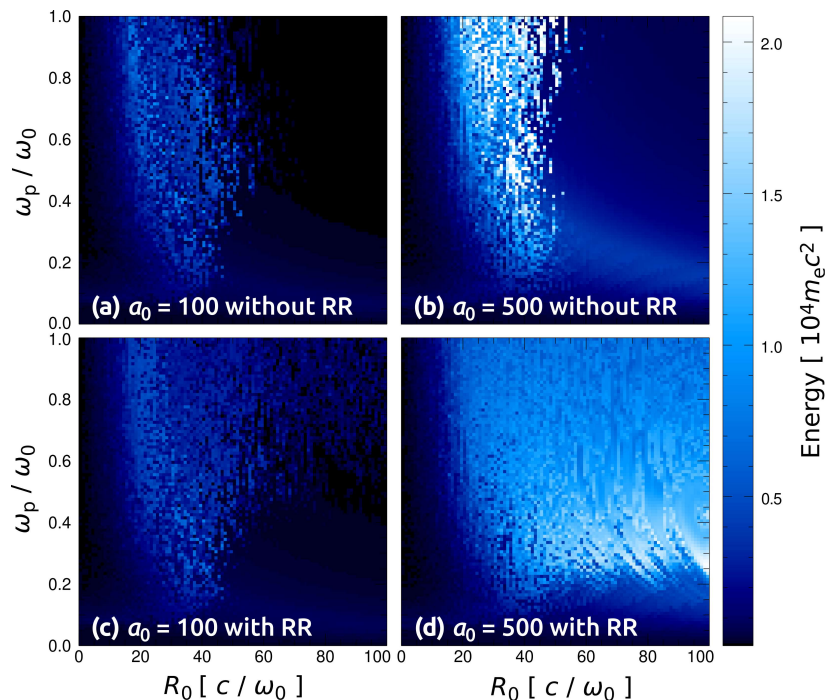


FIG. 6. Maximum electron energy as a function of the normalized plasma frequency ω_p / ω_0 , the initial radial distance R_0 from the channel axis and a_0 . In cases (a) and (b), radiation reaction is neglected, while in cases (c) and (d) it is taken into account.

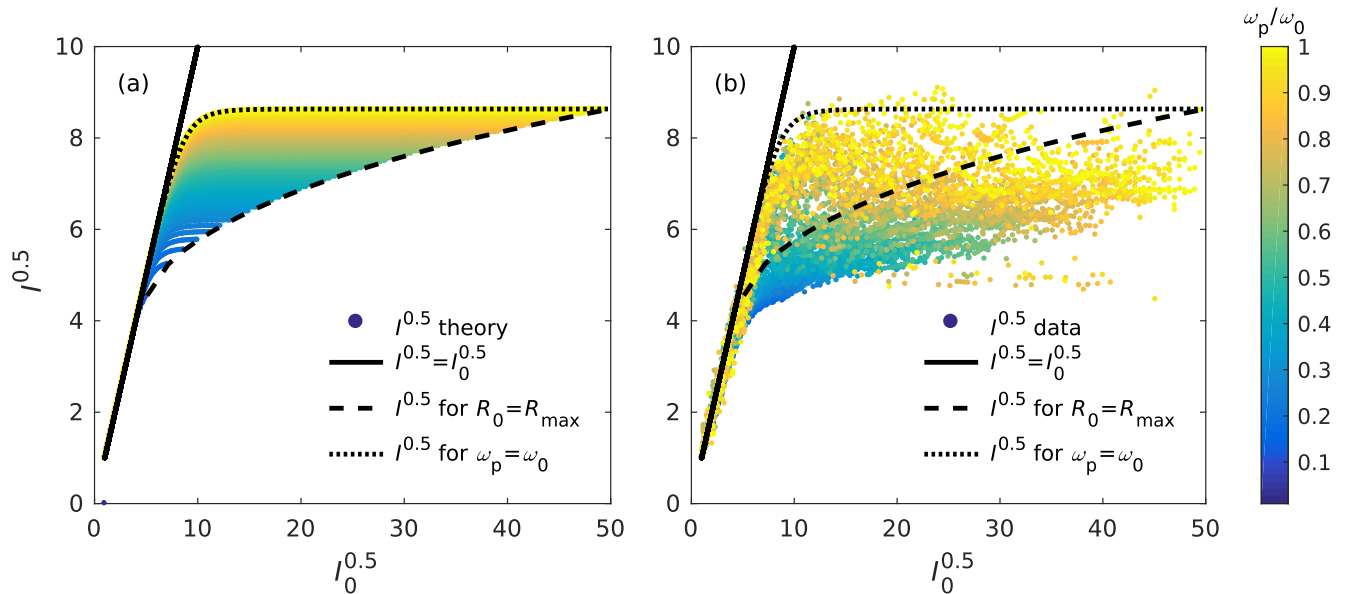


FIG. 7. (a) Theoretical estimate of the reduction of the integral of motion \mathcal{I} after one resonant cycle given by equation (24). (b) Comparison with data points from test-particle simulations at the moment when the electron reaches the maximum energy. The considered laser intensity for both panels corresponds to $a_0 = 500$.

Approximations: limits and validity

We have introduced several approximations in our analytical model, that we hereby justify.

The first question that might arise is that of the choice

of numerical factor f in equation (1) that represents the magnitude of electric versus magnetic field of the channel. The analytical model does not predict changes in the expected energies for any value of f between 0 and 1, and one can verify numerically that this is indeed the case. Examples for $f = 0.5$ and $f = 1.0$ are shown on a param-

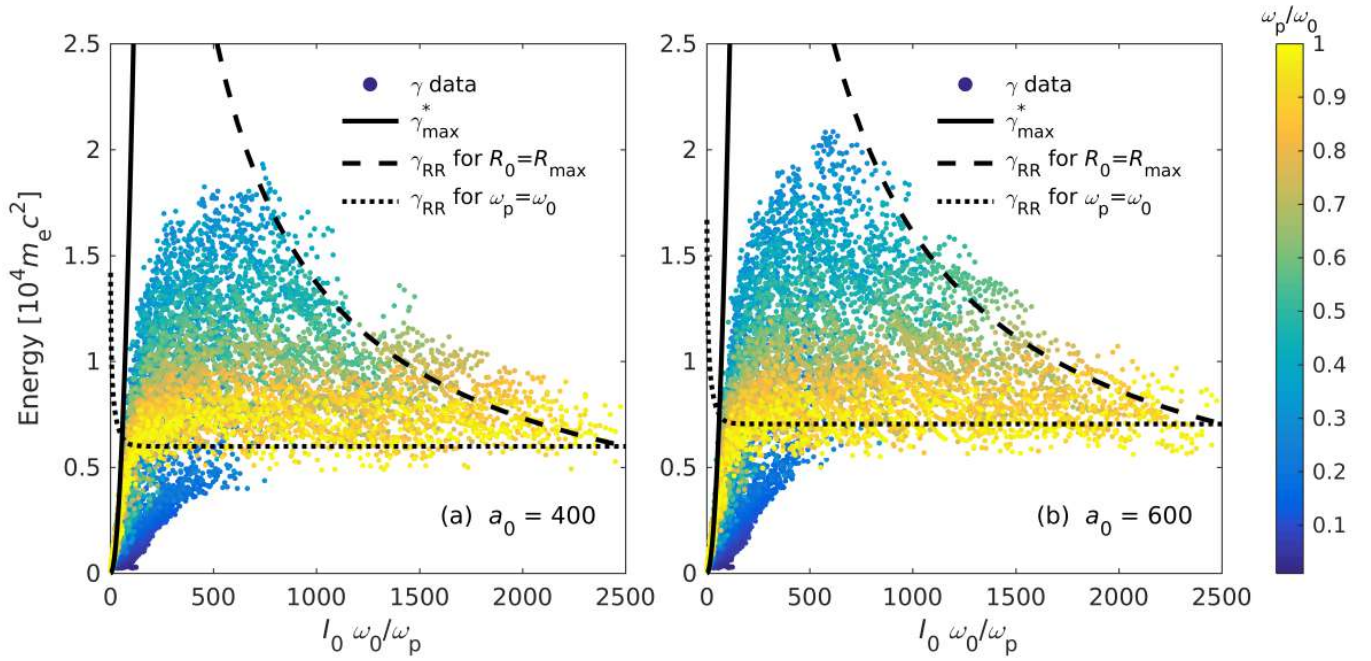


FIG. 8. Summary of parameter studies for (a) $a_0 = 400$ and (b) $a_0 = 600$ with 10^4 test cases varying the plasma frequency ω_p/ω_0 and initial radial electron position R_0 when radiation reaction is taken into account. The solid line corresponds to γ_{\max}^* , equation (9), dashed and dotted line to γ_{RR} , equation (21), for $R_0 = R_{\max} = 100 c/\omega_0$ and for $\omega_p = \omega_0$, respectively.

eter study for $a_0 = 500$ in figure 10 (a) and (b). There are differences for individual test particles (represented by individual pixels), but the expected maximum energy for a given region of parameter space remains unchanged. However, if the electric field turned out to be very low (i.e. $f \rightarrow 0$), particles would need an initial transverse momentum to be efficiently accelerated, because there would be no electrostatic potential in the y -direction.

For simplicity, we have neglected the semi-classical correction to the radiation reaction, modelled by the Gaunt factor $g(\chi_e)$ that reduces the amount of emitted power as a function of parameter χ_e . The parameter χ_e characterizes the interaction of an electron with a strong electromagnetic field [50, 51], and it is approximately equal to the ratio of the field as seen by the electron in its rest frame to the Schwinger limit defined by $E_S = m_e^2 c^3 / (\hbar e)$. Our analysis considered only the leading order term of the radiation reaction, while the correction function is the next order in χ_e [52]. The final electron energies within the channel depend on where the radiation reaction shuts down, and therefore, the most important section of the trajectory should be in the regime where $\chi_e \ll 1$. In that case, the g-factor is a very small correction. We have verified this by introducing the g-factor and showing the expected electron energies on a parameter study for $a_0 = 500$ in figure 10 (c). The differences from results in panel (a) are very small, which confirms this approximation was adequate.

The phase velocity of the laser propagating through

plasma is considered luminal in our model. The actual phase velocity can be expressed as $v_{\text{ph}} \simeq c [1 + n_p / (n_c a_0)]$, where $n_c = \omega_0^2 m_e / (4\pi e^2)$ represents the non-relativistic critical plasma density. This evidently becomes important for dense plasmas and moderate laser intensities. However, as phase difference accumulation between the particle and the wave is an important factor in the acceleration process, there is a possibility that even a small change in the phase velocity of the laser may be relevant for particle dynamics. The luminal approximation is justified as long as the phase accumulation due to the transverse motion of the particle is much larger than the effect of super-luminosity. This is equivalent to stating that the difference between the speed of light and particle average velocity in the direction of laser propagation $c - \langle v_x \rangle$ is much larger than $v_{\text{ph}} - c$. We can estimate using p_x from section I, that $\langle v_x \rangle \simeq c [1 - (1/2)(\langle p_y \rangle / (\gamma m_e c))^2]$ which can be approximated as $\langle v_x \rangle \simeq c [1 - (1/2)(\mathcal{I}/\gamma)]$. To neglect superluminality, the following condition must be met $\mathcal{I}/(2\gamma) \gg (\omega_p/\omega_0)^2/a_0$. As \mathcal{I} reduces, and γ increases over time, the left-hand side of the inequality has a lowest value in the asymptotic conditions, where the particles have reached their maximum allowed energy. We can then use the expression for $\langle \gamma^* \rangle$ from equation (9), as well as $\mathcal{I} \sim 50\sqrt{\omega_p/\omega_0}$ according to equation (24). The condition that must be satisfied then becomes $a_0^2 \gg 5 \times 10^3 (\omega_p/\omega_0)$. The condition is verified for our parameters, which can also be confirmed from figure 10 (d).

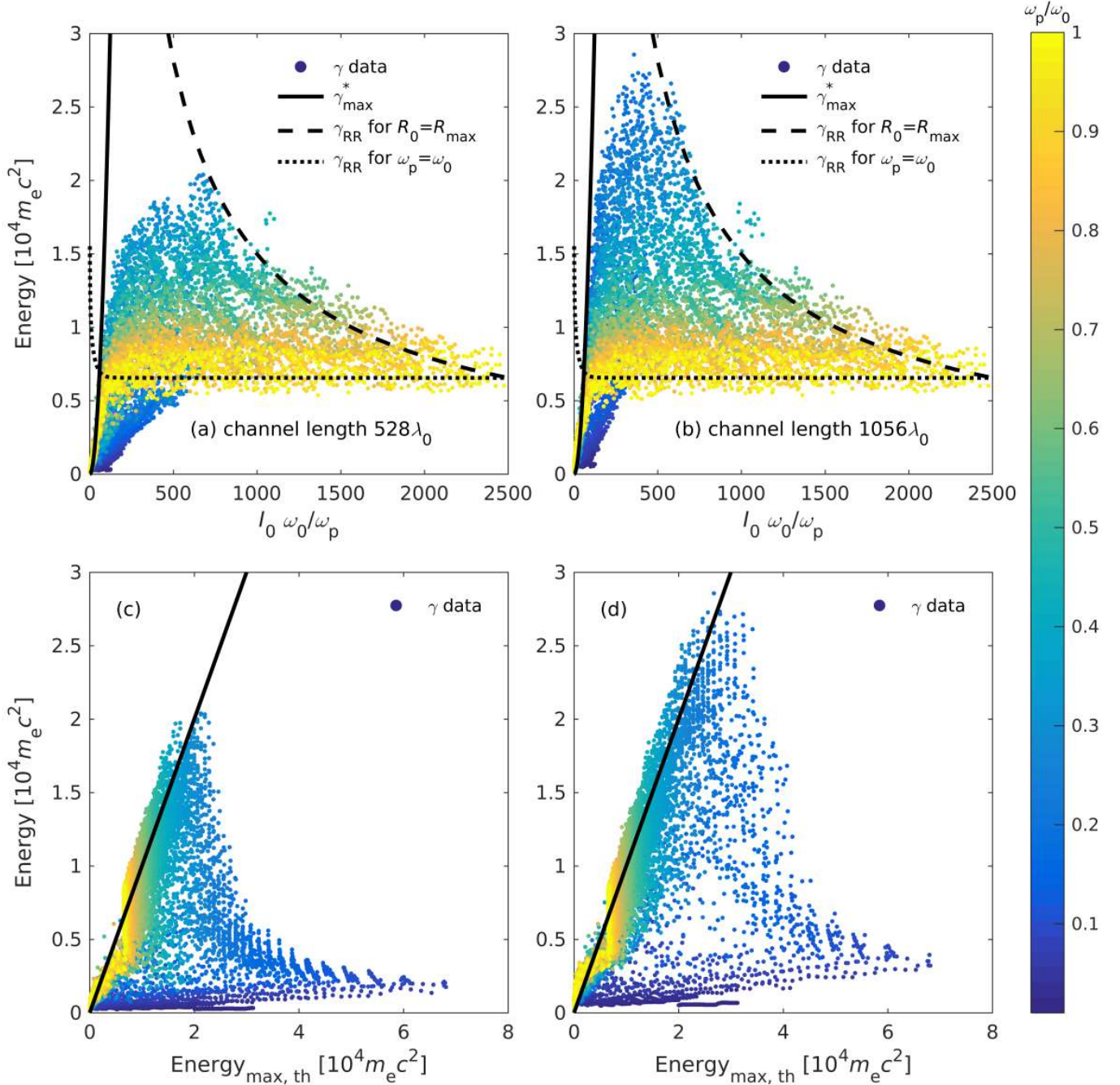


FIG. 9. Maximum electron energy for $a_0 = 500$ in case of (a), (c) 528 μm and (b), (d) 1056 μm long channel. (a), (b) Solid line corresponds to γ_{max}^* , equation (9), dashed and dotted line to γ_{RR} , equation (21), for $R_0 = R_{\text{max}} = 100 c/\omega_0$ and for $\omega_p = \omega_0$, respectively. (c), (d) Achieved energy vs. maximum allowed energy for same datasets as in (a), (b). Solid lines represent cases where the theoretical prediction is equal to the energy attained in the simulations.

Therefore, similarly as in reference [46] we conclude superluminality is a minor effect in our conditions. According to this estimate, for optical lasers $a_0 \gtrsim 300$, the superluminal phase velocity would become important for targets of solid density $n_p \gtrsim 100 n_c$, and negligible for gas jets where $n_p \sim n_c$.

III. PARTICLE-IN-CELL SIMULATIONS

We also compare the maximum electron energy predicted by theory against 2D PIC simulations performed with OSIRIS [53, 54]. We consider several examples of initial conditions for R_0 and ω_p/ω_0 , and two values for the laser intensity $a_0 = 400$ and $a_0 = 600$. The simu-

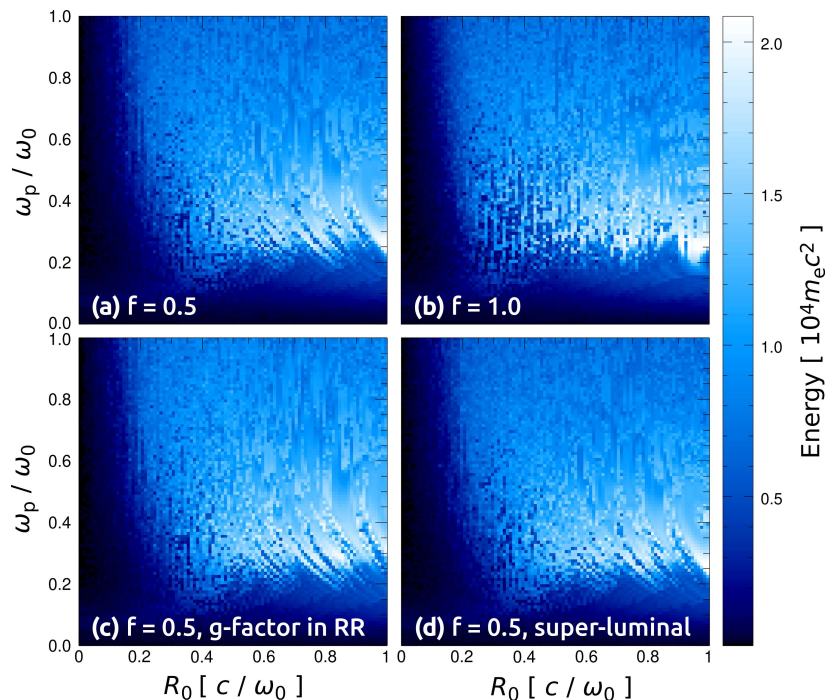


FIG. 10. Maximum electron energy as a function of the normalized plasma frequency ω_p/ω_0 and the initial radial distance R_0 from the channel axis for $a_0 = 500$ with radiation reaction. (a) Parameter f in equation (1) is set to 0.5, the velocity of the wave is luminal and the electron Gaunt factor is not considered. (b) Same as panel (a), except that the value of parameter f is now set to 1.0. (c) Gaunt factor is included in the particle equations of motion, $f = 0.5$, the wave is luminal. (d) The wave is super-luminal, $f = 0.5$, Gaunt factor is neglected.

lation domain for PIC examples was $278 \mu\text{m} \times 286 \mu\text{m}$ resolved with $17\,500 \times 18\,000$ cells. The simulations start with a pre-formed, fully ionized hydrogen plasma channel illustrated in figure 11. Such a channel can be generated by a preceding laser pulse, as presented in reference [44]. The existence of a plasma channel is beneficial for laser guiding and can allow for longer propagation distances than if we rely on self-focusing.

Plasma density at the channel axis is n_p . At the channel radius R_0 , the plasma density reaches its peak $4n_c$, while outside the channel it is set to $2n_c$. The protons are mobile and have the same initial density profile as the electrons. The total length of the plasma slab is $l_{\text{acc}} = 528 \mu\text{m}$, and there is a $5.5 \mu\text{m}$ ramp at the entrance and the exit of the plasma. We use the moving window, and periodic transverse boundary conditions. The laser duration is 150 fs, defined at FWHM in the electromagnetic field amplitude. The transverse profile is Gaussian, with a focal spot radius $W_0 = 3.2 \mu\text{m}$, and the laser wavelength is $\lambda_0 = 1 \mu\text{m}$. Any effects potentially associated with super-luminal phase velocity of the laser are naturally included in the PIC simulations. We will show this later. The radiation reaction is incorporated as follows: for $\chi_e \leq 0.2$ we use the Landau-Lifshitz equation [38] with implementation details given in reference [49]. For $\chi_e > 0.2$ it is modeled with a QED Monte-Carlo based algorithm [55, 56]. The correction to the classical radi-

ation reaction due to the electron Gaunt factor was not considered in the PIC simulations, as it is not expected to affect our conclusions according to Section II.

Energy cutoff

In the following, we compare the highest energy achieved in PIC simulations with the scalings presented in section I. In one PIC simulation, parameters a_0 and ω_p/ω_0 are fixed, but particles can have different R_0 , and the maximum available integral of motion \mathcal{I}_0 will depend on the channel radius and laser spotsize. According to sections I and II, the particles with the maximum initial \mathcal{I}_0 will have the best conditions for acceleration. We therefore use the channel radius to calculate the characteristic \mathcal{I}_0 which gives us the estimate for the expected cutoff energy in a PIC simulation.

Figure 12 shows how maximum energy in the simulation box grows as a function of the propagation distance, both with and without radiation reaction. If radiation reaction is neglected, the electron energy should scale according to equation (13). This trend is confirmed by the results from 2D PIC simulations. However, radiation reaction limits the energy gain. Predictions of equations (9) and (21) are shown together with the data from the 2D PIC simulation with radiation reaction that lies below

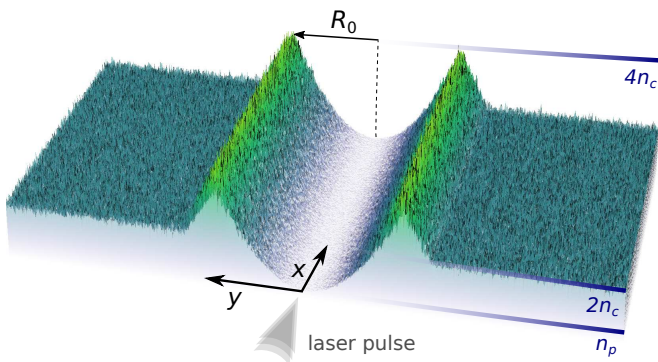


FIG. 11. Transverse profile of the pre-formed plasma channel in PIC simulations. Plasma density at the channel axis is n_p . At the distance R_0 , the plasma density reaches its peak $4n_c$, while outside the channel it is set to $2n_c$, where n_c is the critical plasma density. The incoming laser pulse is propagating along the positive x -direction.

all limits. As expected, the energy cutoff is lower with radiation reaction but the number of accelerated particles is higher. For example, at $t = 210 T_0$, shortly after the radiation reaction effects become visible in global quantities, the simulation with radiation reaction has 2.5 times more particles with energy above 2 GeV than the simulation without radiation reaction, even though the latter has a cutoff energy nearly twice as high.

Among the analytical limits, equation (9) predicts the lowest expected value for the considered parameters. According to our previous analysis, we would expect in this case to have an energy cutoff given by γ_{\max}^* . Instead, the data with radiation reaction converges towards the cycle-averaged value $\langle \gamma^* \rangle$, which is lower. This is not surprising, because our previous analysis considered ideal conditions: the laser transverse intensity distribution was neglected, as well as the energy depletion during propagation. In a realistic setup, particles do not feel the maximum laser intensity everywhere in the channel, and they do not necessarily originate exactly from the edges of the channel. The channel fields are a linear function of R just in a region close to the channel axis, and we have no guarantee that particles initially further than a certain threshold radius would be accelerated because of the finite transverse laser profile. The asymptotic \mathcal{I} can also be lower than the prediction of equation (24) applied to the \mathcal{I}_0 that corresponds to the channel radius. All these effects cannot be formally taken into account for analytical predictions. But if we probe several different combinations of parameters, taking $\langle \gamma^* \rangle$ instead of γ_{\max}^* provides a very good agreement with the energy cutoff measured from 2D PIC simulations. This is shown in figure 13 (a). The energy distribution of the electrons is presented in figure 13 (b). The first two examples illustrate how channel radius changes the electron distribution function. They have the same laser intensity

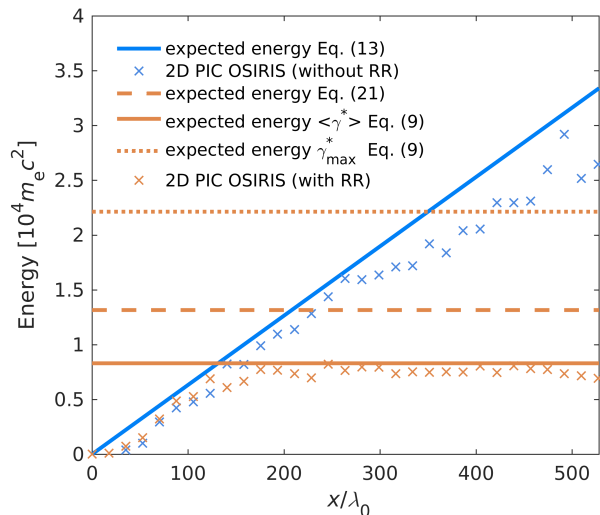


FIG. 12. The maximum electron energy as a function of the propagation distance for the case without (blue) and with (orange) radiation reaction for $\omega_p = 0.5 \omega_0$, $R_0 = 47 c/\omega_0$ and $a_0 = 600$. Solid blue line represents the analytical estimate given by equation (13) without radiation reaction (considering \mathcal{I}_0). Orange lines are obtained using equations (9) and (21) with radiation reaction (considering \mathcal{I} given by equation (24)). Crosses show the corresponding results from 2D PIC simulations.

$a_0 = 600$ and the same background plasma density for which $\omega_p/\omega_0 = 0.5$, but the channel radius changes by a factor of two. The energy cutoff does not change significantly, which suggests that the narrower channel is wide enough for electrons to achieve the maximum allowed energy. However, the number of particles that approach this value is significantly higher in the case with the wider channel, which is reflected on the slope of the spectrum. Other examples show that the cutoff can be increased by reducing the plasma density. The optimal initial distance from the axis depends on the plasma density according to equation (14), so reducing the density to $\omega_p/\omega_0 = 0.32$ does not increase much the energy cutoff if the channel radius remains small $R_0 = 47 c/\omega_0$. However, if one combines the wider channel with the lower plasma density, the electron energy cutoff evidently increases. By applying this strategy, it is possible to obtain more energetic electrons even using lower laser intensities (e.g. $a_0 = 400$ in figure 13).

The electromagnetic field structure

We proceed to a more detailed analysis of PIC results, to illustrate the connection with the analytical model presented in Section I. In figure 14 we present density and field profiles for a simulation with parameters $\omega_p = 0.27 \omega_0$, $R_0 = 81 c/\omega_0$ and $a_0 = 600$ at time

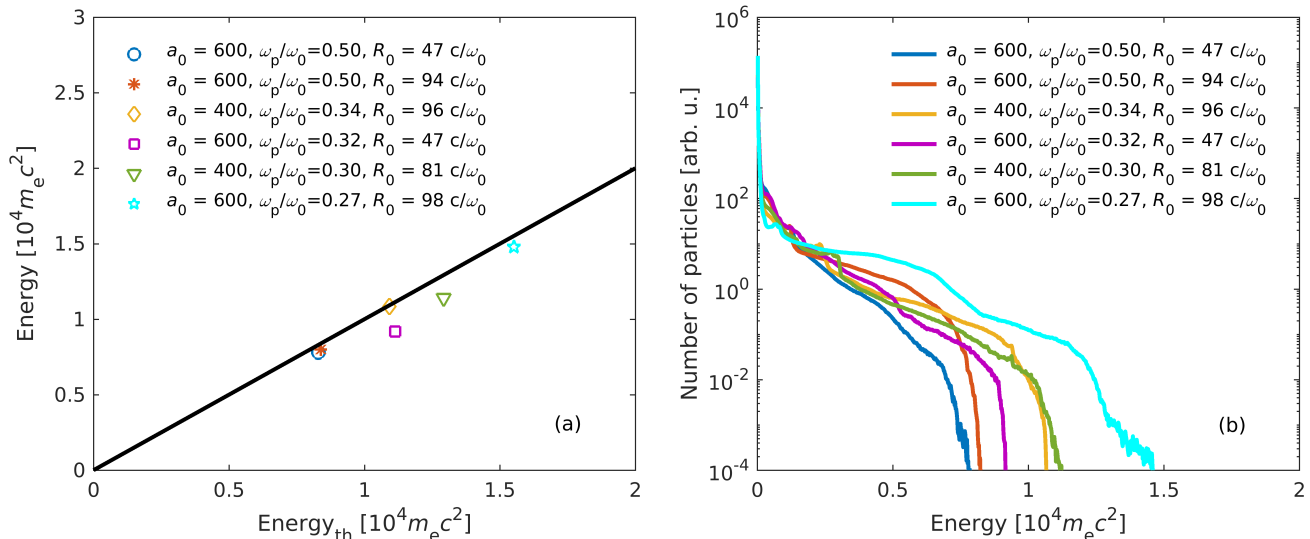


FIG. 13. (a) Achieved energy in PIC simulations vs. theoretical expectation. The theoretical prediction is obtained by taking a minimum predicted value using equation (21), $\langle \gamma^* \rangle$ from equation (9) and equation (13). Solid line represents cases where the theoretical prediction is equal to the energy attained in the simulations. (b) Electron energy distribution at the end of the channel in corresponding PIC simulations.

$t = 2501 \omega_0^{-1}$. Panels (a) and (c) show density profiles of ions and electrons during the propagation of the laser pulse depicted in panel (e). The detailed structure of the electromagnetic field within the smaller box marked in (e) is presented in panels (b), (d) and (f). Inside the channel, the laser is partially absorbed, but the wavefronts are nearly straight, as can be verified by observing the transverse electromagnetic field components E_y and B_z . The longitudinal electric field E_x generated by the density fluctuations within the channel is noisy, and can potentially work towards or against acceleration of individual particles. Panels (g) and (h) show the total focusing field associated with the plasma channel, given by equation (1). As these fields are weaker than the laser field, one can obtain only the total value $|E_C| + |B_C|$ by subtracting $E_y - B_z$. Doing so reveals a long-range field structure, linearly dependent on the distance from the axis. The amplitude of the focusing field is of the same order as E_x , with a difference that the E_x average is close to zero on scales larger than a laser wavelength. The color-coded lineouts in panel (h) confirm that the channel field can be regarded as a linear function of the distance from the axis up to approximately $R_0/2$, where the slope is defined by the effective plasma density. For a flat density plasma slab, the effective density is the background plasma density n_p . For a channel with a parabolic density gradient like ours, the average plasma density for the region around the channel axis between $-R_0/2$ and $R_0/2$ can be calculated analytically and directly applied to equations presented in Section I. The channel field predicted by equation (1) using the effective plasma density $n_p^{\text{eff}} \simeq 0.4 n_c$ is illustrated by the black dashed line in

panel (h) which is in agreement with the value extracted from the PIC simulation.

Particle motion

For the same simulation parameters, figure 15 shows randomly selected trajectories among particles that achieved energies $\xi > 10^4 m_e c^2$ at $t = 2501 \omega_0^{-1}$ (the same time shown in figure 14). The trajectories are color-coded in energy, showing the configuration space along with the evolution of transverse and longitudinal momenta vs. the longitudinal x -position.

Laser-electron dephasing depends on the velocity of the particle along the laser propagation direction β_x and phase velocity of the laser. One can measure the phase velocity in PIC simulations from the temporal evolution of the electric field along the channel axis, shown in panel (g). The phase velocity is not constant, owing to the 2D laser dynamics. The measured average phase velocity is $1.00075c$, on the same order as the analytical prediction in Section II that gives the value $1.00066c$ for our $n_p^{\text{eff}} \simeq 0.4 n_c$ and $a_0 = 600$. The β_x depends on the ratio $p_y/p_x \sim 0.1$ (c. f. figure 15), which confirms that for resonant particles the transverse electron motion has about an order of magnitude stronger effect on dephasing than superluminality (and more than one order of magnitude for non-resonant particles). We can therefore apply our analytical model for studying the particle motion.

Figure 15 shows the particles perform a similar asymptotic motion at late times, despite the different initial dynamics. Some particles achieve resonance faster than

others. The interaction with the laser can start from rest, or after pre-acceleration at the laser-plasma interface. The integral of motion associated with the initial distance $R_0/2$ from the axis is $\mathcal{I}_0 \sim 160$. According to equation (24), the expected integral of motion \mathcal{I} after one full resonant cycle would be $\mathcal{I} \sim 60$, while after two cycles $\mathcal{I} \sim 50$. Among our selected particles, there are many that completed two full resonant cycles. The temporal evolution of trajectories in p_y -energy phase-space is also shown, with a highlighted single-particle example in panel (d). This illustrates how the most energetic particles gain energy over time: they first oscillate in the region of low energy, unable to retain the energy gained over the oscillation cycle; as the oscillations become quasi-resonant, the particles can retain a fraction of the energy obtained, and they accelerate sloshing back and forth from the points on the parabola defined by their current integral of motion through $p_y = m_e c \sqrt{2\gamma\mathcal{I}}$. The definition of the parabola follows from equation (6) when $\cos\psi \simeq 1$. The phase-space associated with simulation particles initially at rest within the channel between $680 < x * \omega_0/c < 725$ is shown in panels (f) and (h) for times $t = 2501 \omega_0^{-1}$ and $t = 4000 \omega_0^{-1}$, respectively. The colorscale is logarithmic, to highlight all possible combinations of p_y and energy. The widest parabola is associated with the maximum initial integral of motion $\mathcal{I}_0 = 160$ available among the considered particles. As the time passes, the invariant \mathcal{I} of some particles can be reduced. The two inner parabolas show the asymptotic value after one (dashed line) and two (solid line) resonant cycles. The energetic particles are eventually expected inside the parabola associated with the asymptotic \mathcal{I} , as shown in panel (h). According to equation (20), the expected asymptotic value of the Lorentz factor for $\mathcal{I} = 50$ is $\gamma \sim 1.1 \times 10^4$. We can also predict the amplitude of oscillations around the channel axis for these particles is about $22 c/\omega_0$ by inserting $p_y = 0$ in equation (6). All these estimates are in agreement with our simulation results.

IV. CONCLUSIONS

The betatron resonance in a plasma channel can result in efficient electron acceleration, but strongly depends on the initial particle position, channel density, laser intensity and acceleration distance. Particles with an initial radius $R_0 \simeq R_{\text{opt}}$, where R_{opt} is defined by equation (14), have the best chance to attain the maximum energy in the system. At very high laser intensities, radiation reaction causes a decrease in the maximum electron energy, however, it allows accelerating a higher number of particles as it affects the phase-matching process between betatron and laser oscillations. In fact, nearly all particles with $R_0 > R_{\text{opt}}$ have a very good chance to be accelerated due to radiation reaction, provided that R_{opt}

is still within the range where channel fields are nearly a linear function of the distance from the laser propagation axis. To that end, it may be optimal to use plasma channel radius $\sim 2R_{\text{opt}}$.

Analytical predictions of the maximum electron energy as a function of channel density and electron initial radial position are provided by equations (9) and (21) using radiation-reaction reduced value of \mathcal{I} given by the lowest estimate from equations (24) and (25). The required acceleration distance to achieve this energy can be estimated through equation (13). Our findings are confirmed by numerical integration of test particle trajectories, as well as 2D full-scale PIC simulations. According to the presented calculations, using near-future lasers (10 PW-class, 150 fs) we can obtain multi-GeV electrons in a single-stage acceleration within a 0.5 mm-long plasma channel. We envisage a roadmap towards electron energies in excess of 10 GeV if the channel and laser parameters are matched for an optimal outcome.

Our findings can be extended to acceleration of externally injected beams, with an arbitrary beam loading (i.e. high current within the channel, similar as in reference [46]). In that case, the background magnetic field due to the current within the channel may be stronger than expected from the background plasma density. For such a setup, one should estimate an effective (higher) value for the plasma density n_p^{eff} that would correspond to a comparable current density and the same order of magnitude for the self-consistent background magnetic field within the plasma. Our scaling laws can then be applied using this effective n_p^{eff} instead of n_p to calculate the asymptotic cutoff energy of the electron beam. An example for $a_0 = 200$ and $a_{MB} = 10^{-2}a_0$ from reference [46], can be mapped using $\mathcal{I} \sim 40$ and $\omega_p/\omega_0 \sim 0.3$. Our model predicts the asymptotic electron energy is ~ 7 GeV, which is in agreement with their simulations that show 7.5 GeV.

ACKNOWLEDGEMENTS

This work was supported by the European Research Council (ERC-2015-AdG Grant No. 695088), Portuguese Science Foundation (FCT) Grant No. SFRH/BPD/119642/2016 and by the project High Field Initiative (CZ.02.1.01/0.0/0.0/15_003/0000449) from European Regional Development Fund (HiFI). The support of Czech Science Foundation project No. 18-09560S is acknowledged. The results of the Project LQ1606 were obtained with the financial support of the Ministry of Education, Youth and Sports as part of targeted support from the National Programme of Sustainability II. We acknowledge PRACE for awarding access to MareNostrum based in the Barcelona Supercomputing Center. The simulations were performed at MareNostrum (Spain), IST Cluster (Portugal) and ECLIPSE (ELI Beamlines,

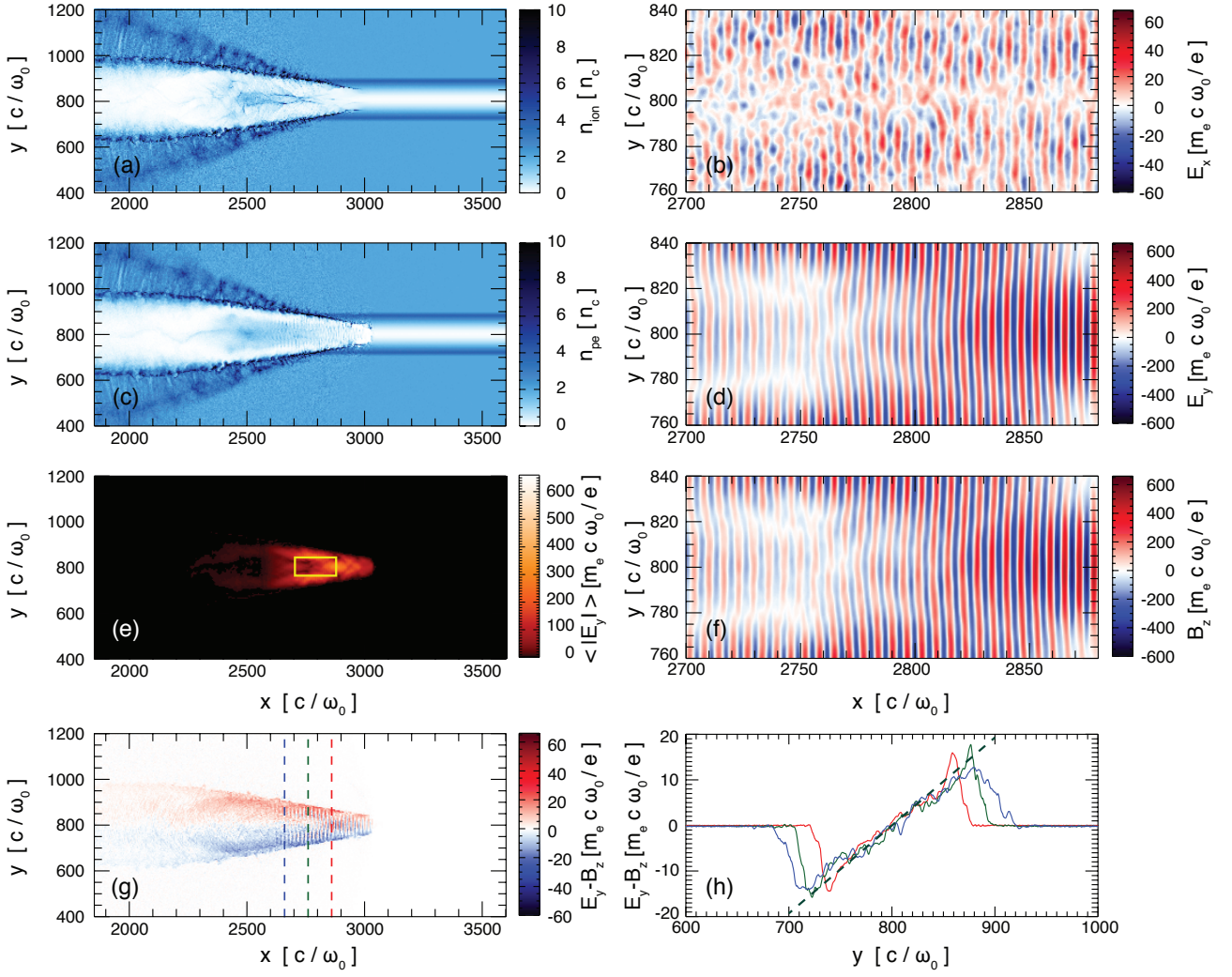


FIG. 14. Results from PIC for $\omega_p = 0.27 \omega_0$, $R_0 = 81 c/\omega_0$ and $a_0 = 600$ at time $t = 2501 \omega_0^{-1}$. (a) Proton density, (c) electron density, (e) average absolute value of transverse electric field, (b) longitudinal electric field, (d) transverse electric field, (f) transverse magnetic field, (g) background channel field obtained by subtracting $E_y - B_z$ and (h) lineouts of the channel field. The black dashed line in panel (h) represents the expected channel field according to equation (1) using $n_p^{\text{eff}} \simeq 0.4 n_c$.

Czech Republic).

-
- [1] Tajima T and Dawson J M 1979 *Phys. Rev. Lett.* **43** 267
[2] Faure J, Glinec Y, Pukhov A, Kiselev S, Gordenko S, Lefebvre E, Roesseau J P, Burgy F and Malka V 2004 *Nature* **431** 541–544
[3] Geddes C G R, Toth C, Tilborg J V, Esarey E, Schroeder C B, Bruhwiler D, Nieter C, Cary J and Leemans W P 2004 *Nature* **431** 538–541
[4] Mangles S P D, Murphy C D, Najmudin Z, Thomas A G R, Collier J L, Dangor A E, Dival E J, Foster P S, Gallacher J G and Hooker C J 2004 *Nature* **431** 535–538

- [5] Leemans W, Gonsalves A, Mao H S, Nakamura K, Benedetti C, Schroeder C, Tóth C, Daniels J, Mittelberger D, Bulanov S, Vay J L, Geddes C and Esarey E 2014 *Phys. Rev. Lett.* **113** 245002
[6] Gonsalves A, Nakamura K, Daniels J, Benedetti C, Pieronek C, de Raadt T, Steinke S, Bin J, Bulanov S, van Tilborg J, Geddes C, Schroeder C, Tóth C, Esarey E, Swanson K, Fan-Chiang L, Bagdasarov G, Bobrova N, Gasilov V, Korn G, Satorov P and Leemans W 2019 *Phys. Rev. Lett.* **122** 084801
[7] Pukhov A, Sheng Z M and ter Vehn J M 1999 *Phys. Plasmas* **6** 2847–2854
[8] Tsakiris G D, Gahn C and Tripathi V K 2000 *Phys. Plasmas* **7** 3017–3030
[9] Qiao B, He X T, ping Zhu S and Zheng C Y 2005 *Phys. Plasmas* **12** 083102

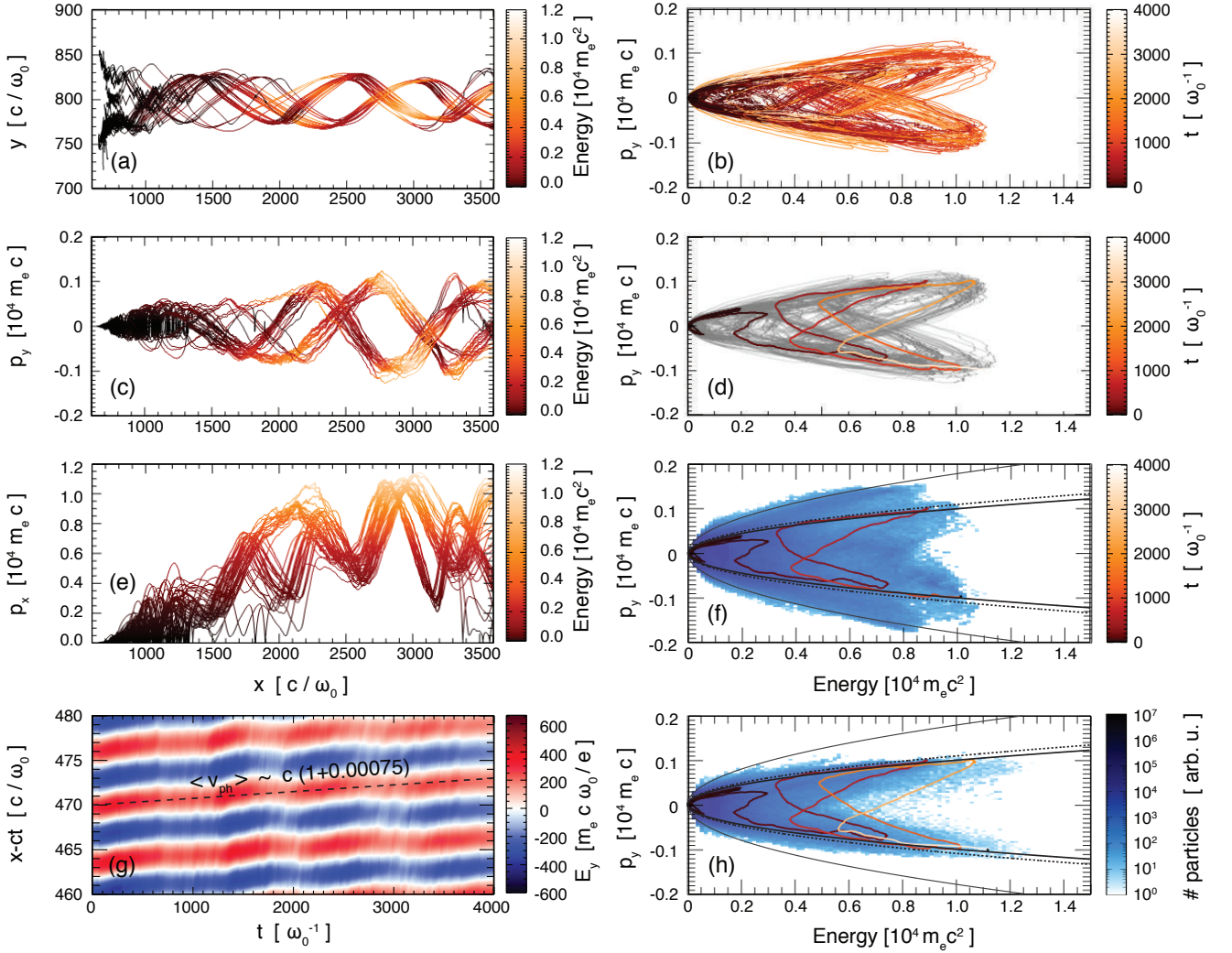


FIG. 15. Results from PIC for $\omega_p = 0.27 \omega_0$, $R_0 = 81 c/\omega_0$ and $a_0 = 600$. (a) Trajectory, (c) transverse and (e) longitudinal momenta of 48 randomly selected electrons with energy above $10^4 m_e c^2$ at $t = 2501 \omega_0^{-1}$. Panels (b, d, f, h) show the time evolution of the electrons in p_y -energy phase-space. Panel (d) highlights the trajectory of one efficiently accelerated electron. This trajectory is overlaid with the p_y -energy phase-space (blue scale) and analytical estimates for the connection between p_y and energy when betatron phase is $\cos \psi \simeq 1$ (the point of local maximum for p_y) in panels (f) $t = 2501 \omega_0^{-1}$ and (h) $t = 4000 \omega_0^{-1}$. The outer solid line is associated with the highest initial integral of motion in the system, while the inner lines show the expected values after one (dotted line) and two (solid line) resonant cycles according to equation (24). Panel (g) shows time evolution of the transverse electric field along the x -axis inside a simulation window moving at the speed of light. The figure represents a magnified portion of space slightly over three wavelengths long, such that phase velocity can be measured directly.

- [10] Qiao B, ping Zhu S, Zheng C Y and He X T 2005 *Phys. Plasmas* **12** 053104
- [11] Li Y Y, Gu Y J, Zhu Z, Li X F, Ban H Y, Kong Q and Kawata S 2011 *Phys. Plasmas* **18** 053104
- [12] Gu Y J, Kong Q, Li Y Y, Ban H Y, Zhu Z and Kawata S 2011 *Phys. Plasmas* **18** 030704
- [13] Liu B, Wang H Y, Liu J, Fu L B, Xu Y J, Yan X Q and He X T 2013 *Phys. Rev. Lett.* **110** 045002
- [14] Shaw J L, Tsung F S, Vafaei-Najafabadi N, Marsh K A, Lemos N, Mori W B and Joshi C 2014 *Plasma Phys. Control. Fusion* **56** 084006
- [15] Robinson A P L, Arefiev A V and Khudik V N 2015 *Phys. Plasmas* **22** 083114
- [16] Hu R, Liu B, Lu H, Zhou M, Lin C, Sheng Z, Chen C, He X and Yan X 2015 *Sci. Rep.* **5** 15499
- [17] Arefiev A V, Khudik V N, Robinson A P L, Shvets G, Willingale L and Schollmeier M 2016 *Phys. Plasmas* **23** 056704
- [18] Khudik V, Arefiev A, Zhang X and Shvets G 2016 *Phys. Plasmas* **23** 103108

- [19] Arefiev A V, Khudik V N, Robinson A P L, Shvets G and Willingale L 2016 *Phys. Plasmas* **23** 023111
- [20] Zhang R, Cheng L H, Tang R A and Xue J K 2016 *Phys. Plasmas* **23** 093105
- [21] Huang T W, Robinson A P L, Zhou C T, Qiao B, Liu B, Ruan S C, He X T and Norreys P A 2016 *Phys. Rev. E* **93** 063203
- [22] Huang T W, Zhou C T, Zhang H, Wu S Z, Qiao B, He X T and Ruan S C 2017 *Phys. Rev. E* **95** 043207
- [23] Jiang K, Zhou C T, Huang T W, Wu C N, Ju L B, Zhang H, Wu S Z, Cai T X, Qiao B, Yu M Y and Ruan S C 2018 *Phys. Rev. E* **98** 033206
- [24] Geng P F, Lv W J, Li X L, Tang R A and Xue J K 2018 *Chin. Phys. B* **27** 035201
- [25] Wang T, Khudik V, Arefiev A and Shvets G 2019 *Phys. Plasmas* **26** 083101
- [26] Arefiev A V, Breizman B N, Schollmeier M and Khudik V N 2012 *Phys. Rev. Lett.* **108** 145004
- [27] Arefiev A V, Khudik V N and Schollmeier M 2014 *Phys. Plasmas* **21** 033104
- [28] Arefiev A V, Robinson A P L and Khudik V N 2015 *J. Plasma Phys.* **81** 475810404
- [29] Huang T W, Zhou C T, Robinson A P L, Qiao B, Arefiev A V, Norreys P A, He X T and Ruan S C 2017 *Phys. Plasmas* **24** 043105
- [30] Robinson A P L, Arefiev A V and Neely D 2013 *Phys. Rev. Lett.* **111** 065002
- [31] Khudik V N, Zhang X, Wang T and Shvets G 2018 *Phys. Plasmas* **25** 083101
- [32] Robinson A P L and Arefiev A V 2017 *Phys. Plasmas* **24** 023101
- [33] Gahn C, Tsakiris G D, Pukhov A, ter Vehn J M, Pretzler G, Thirof P, Habs D and Witte K J 1999 *Phys. Rev. Lett.* **83** 4772
- [34] Mangles S P D, Walton B R, Tzoufras M, Najmudin Z, Clarke R J, Dangor A E, Evans R G, Fritsler S, Gopal A, Hernandez-Gomez C, Mori W B, Rozmus W, Tatarakis M, Thomas A G R, Tsung F S, Wei M S and Krushelnick K 2005 *Phys. Rev. Lett.* **94** 245001
- [35] Weber S, Bechet S, Borneis S, Brabec L, Bucka M, Chacon-Golcher E, Ciappina M, DeMarco M, Fajstavr A, Falk K, Garcia E R, Grosz J, Gu Y J, Hernandez J C, Holec M, Janecka P, Jantac M, Jirka M, Kadlecova H, Khikhlikha D, Klimo O, Korn G, Kramer D, Kumar D, Lastovicka T, Lutoslawski P, Morejon L, Olsovcova V, Rajdl M, Renner O, Rus B, Singh S, Smid M, Sokol M, Versaci R, Vrana R, Vranic M, Vyskocil J, Wolf A and Yu Q 2017 *Matter Rad. Extremes* **2** 149
- [36] Gales S, Balabanski D L, Negoita F, Tesileanu O, Ur C A, Ursescu D and Zamfir N V 2016 *Phys. Scr.* **91** 093004
- [37] Zou J, Blanc C L, Papadopoulos D, Chériaux G, Georges P, Mennerat G, Druon F, Lecherbourg L, Pellegrina A, Ramirez P, Giambruno F, Fréneaux A, Leconte F, Badarau D, Boudenne J, Fournet D, Valloton T, Paillard J, Veray J, Pina M, Monot P, Chambaret J, Martin P, Mathieu F, Audebert P and Amiranoff F 2015 *High Power Laser Science and Engineering* **3**
- [38] Landau L D and Lifshitz E M 1975 *The classical theory of fields* Pergamon international library of science, technology, engineering, and social studies (Pergamon Press)
- [39] Qiao B, Chang H X, Xie Y, Xu Z and He X T 2017 *Phys. Plasmas* **24** 123101
- [40] Chang H X, Qiao B, Huang T W, Xu Z, Zhou C T, Gu Y Q, Yan X Q, Zepf M and He X T 2017 *Sci. Rep.* **7** 45031
- [41] Huang T W, Zhou C T, Zhang H, Wu S Z, Qiao B, He X T and Ruan S C 2017 *Appl. Phys. Lett.* **110** 021102
- [42] Wang T, Gong Z, Chin K and Arefiev A 2019 *Plasma Phys. Control. Fusion* **61** 084004
- [43] Ji L L, Pukhov A, Kostyukov I Y, Shen B F and Akli K 2014 *Phys. Rev. Lett.* **112** 145003
- [44] Vranic M, Fonseca R A and Silva L O 2018 *Plasma Phys. Control. Fusion* **60** 034002
- [45] Liu C, Shen B, Zhang X, Ji L, Bu Z, Wang W, Yi L, Zhang L, Xu J, Xu T and Pei Z 2018 *Phys. Plasmas* **25** 023107
- [46] Gong Z, Mackenroth F, Yan X Q and Arefiev A V 2019 *Sci. Rep.* **9** 17181
- [47] Pukhov A 2002 *Rep. Prog. Phys.* **66** 47
- [48] Arefiev A V, Cochran G E, Schumacher D W, Robinson A P L and Chen G 2016 *AIP Conf. Proc.* **1777** 050001
- [49] Vranic M, Martins J, Fonseca R and Silva L 2016 *Comput. Phys. Commun.* **204** 141
- [50] Nikishov A and Ritus V 1964 *Sov. Phys. JETP* **19** 529
- [51] Zeldovich Y B 1975 *Sov. Phys. Uspekhi* **18** 79
- [52] Ritus V I 1985 *J. Sov. Laser Res.* **6** 497–617
- [53] Fonseca R A, Silva L O, Tsung F S, Decyk V K, Lu W, Ren C, Mori W B, Deng S, Lee S, Katsouleas T and Adam J C 2002 Osiris: A three-dimensional, fully relativistic particle in cell code for modeling plasma based accelerators *Computational Science — ICCS 2002* ed Sloat P M A, Hoekstra A G, Tan C J K and Dongarra J J (Springer Berlin Heidelberg) pp 342–351
- [54] Fonseca R A, Vieira J, Fiuza F, Davidson A, Tsung F S, Mori W B and Silva L O 2013 *Plasma Phys. Control. Fusion* **55** 124011
- [55] Grismayer T, Vranic M, Martins J L, Fonseca R A and Silva L O 2016 *Phys. Plasmas* **23** 056706
- [56] Grismayer T, Vranic M, Martins J L, Fonseca R A and Silva L O 2017 *Phys. Rev. E* **95** 023210